Optimization of imaging techniques for background suppression of stellar Nucleo-Synthesis reactions with i-TED

Characterization, Upgrades and Outlook

Bernardo Gameiro (IFIC), Jorge Lerendegui Marco (IFIC), James Hallam (IFIC), Javier Balibrea Correa (IFIC), Ion Ladarescu (IFIC), César Domingo Pardo (IFIC), Víctor Babiano Suárez (UV)

Red Temática de Física Nuclear
XV CPAN days, Octuber 2-6 2023, Santander

2023/10/03

Motivation

- **Neutron capture cross-section measurements:**
  - **Astrophysical interest:**
    - s-process of nucleosynthesis
  - **Typical experiment:**
    - Neutron time of flight
  - **Major challenges:**
    - Direct neutron background
    - Neutron-induced background

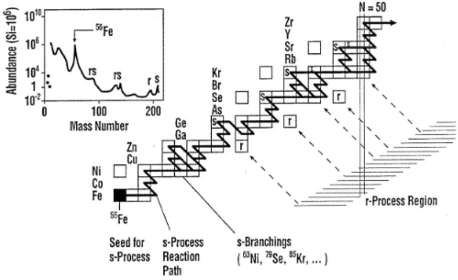

Figure 1: Scheme of the neutron-capture processes, including the s-process path, relevant for the motivation of the present work.

Motivation

- **Neutron capture cross-section measurements:**
  - **Astrophysical interest:**
    - s-process of nucleosynthesis
  - **Typical experiment:**
    - Neutron time of flight
  - **Major challenges:**
    - Direct neutron background
    - Neutron-induced background

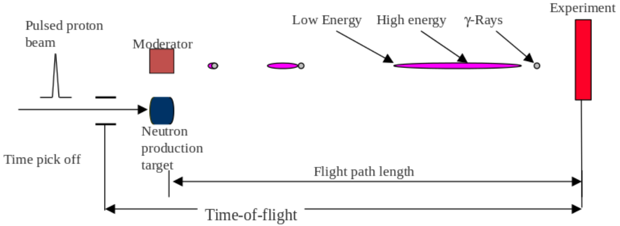

Figure 2: Scheme of a neutron time of flight experiment.

Motivation

- **Neutron capture cross-section measurements:**
  - **Astrophysical interest:**
    - s-process of nucleosynthesis
  - **Typical experiment:**
    - Neutron time of flight
  - **Major challenges:**
    - Direct neutron background
    - Neutron-induced background

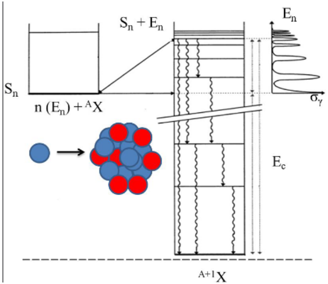

Figure 3: Scheme of a neutron capture to an excited state and possible decays to ground state by emission of different γ-ray cascades.

Major challenges

- **Direct neutron background:**
  - Neutrons scattered on the target
  - Detector requirement: $\downarrow$ neutron sensitivity
- **Neutron-induced γ background:**
  - Neutrons interact with environment
  - Detector requirement: select γ events

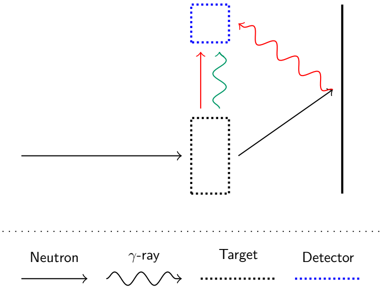

Figure 4: Possible interactions.

Solution

- **Imaging:**
  - Select events based on spatial origin
  - i-TED
    - Total-energy detector
    - Imaging capabilities
    - Compton camera
- **Main features:**
  - Different requirements sometimes pull development in opposing ways

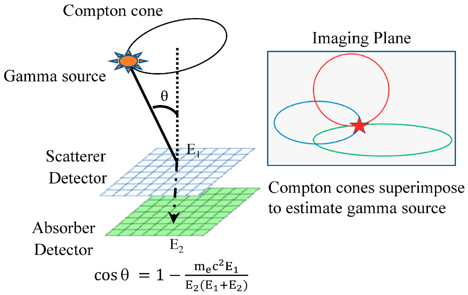

Figure 5: Working principle of a Compton camera.

Detectors: Multi i-TED Array

- **i-TED modules** $\times 4$:
  - 2 planes per module
  - 1+4 crystals+SiPM per module
  - 8×8 pixels per SiPM
  - Total of 1280 channels!
- **Innovative system:**
  - Currently C_6D_6 are used
  - Adds spatial discrimination for γ-rays
  - Adds complexity to the system
- **Current status:**
  - Years of development
  - First experimental results of $^{79}Se(n, \gamma)$
  - Working, optimized, characterized

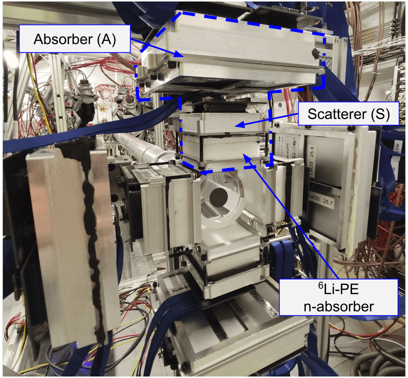

Figure 6: Multi i-TED detector system in its first experimental campaign.

Detectors: i-TED-E Module

- New addition to the lab!
- For testing and applications:
  - Range verification in hadrontherapy
  - Nuclear waste verification
  - Dosimetry in boron-neutron capture therapy
  - Radio-guided surgery
- Enter i-TED-E:
  - Working, characterized
  - First experimental campaign (CMAM 2023/06)
  - Upcoming experimental campaign (ILL 2023/10)

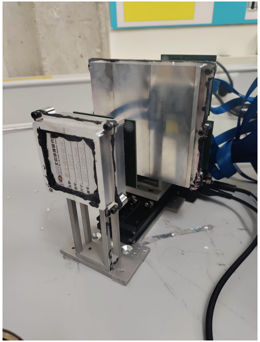

Figure 7: i-TED-E with its full metal casing and without the ^{6}Li neutron shield

Major Detector Upgrades

Irregular pixelmaps

Noise from $\neq$ gains

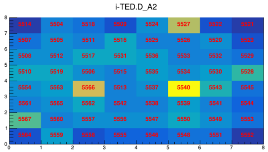

ASIC temperature

Thermal gain drift

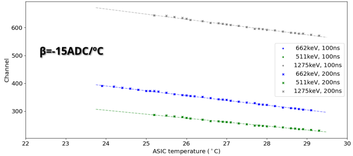

CRT study

PET mode

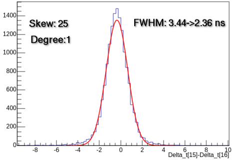

Per-pixel threshold

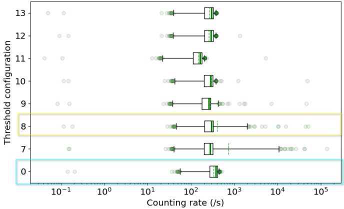

Temperature correction

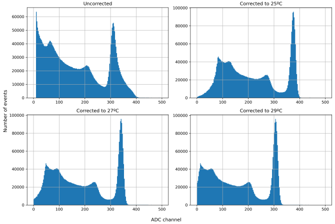

Compton mode

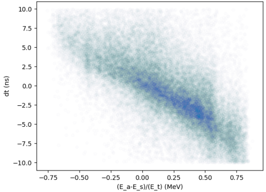

Imaging algorithms

- **Algorithms:**
  - Back-projection
  - Analytical
  - Stochastic Origin Ensemble
- **Back-projection:**
  - Origin probability
  - Simple & fast
  - Smooth peak
- **Analytical:**
  - Origin probability
  - Better peak to background ratio
  - Artifacts

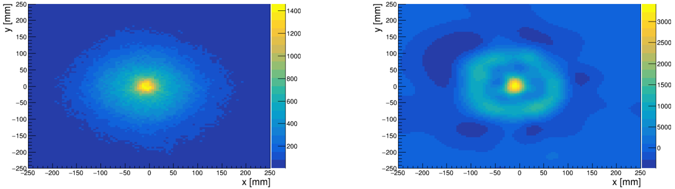

(a) Back-projection (b) Analytical

Figure 8: Comparison of results of different imaging algorithms.

Position sensitivity

- Clear spatial difference

Method	Position	X-Centroid	σ_X	Y-Centroid	σ_Y
BP	(-50,0)	-36.0	36.2	0.7	37.6
Analytical	(-50,0)	-65.3	21.6	3.6	16.0
BP	(0,50)	-8.2	17.4	32.7	23.5
Analytical	(0,50)	-11.1	14.1	41.8	16.3
BP	(0,0)	-6.3	24.0	-0.9	22.8
Analytical	(0,0)	-8.9	18.8	0.4	24.0

Table 1: Deviation and resolution (in mm) of the back-projection and analytical algorithms for Compton imaging. Study of ^{22}Na source in different positions.

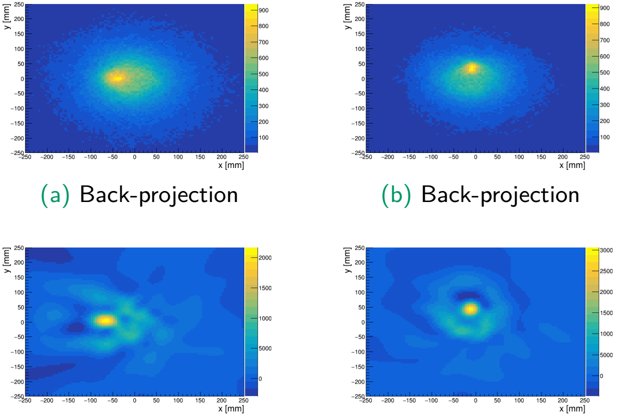

(a) Back-projection (b) Back-projection

(c) Analytical (d) Analytical

Figure 9: Position sensitivity with different algorithms.

Effect of focal distance

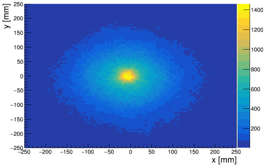

(a) Back-projection 10

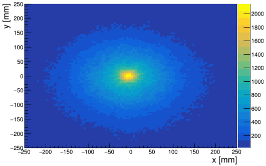

(b) Back-projection 30

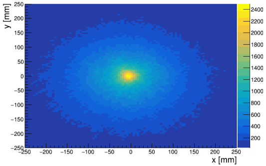

(c) Back-projection 40

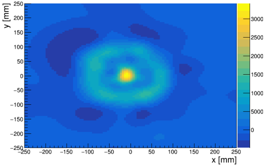

(d) Analytical 10

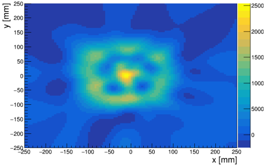

(e) Analytical 30

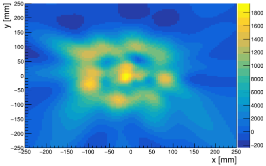

(f) Analytical 40

Figure 10: Effect of focal distance

Figures of Merit and Validation

- **Objective:**
  Spatial cuts
- **Problem:**
  Imaging doesn't give coordinates
- **Solution:**
  Need for other figures of merit
- **Validation:**
  Experimentally verify applicability

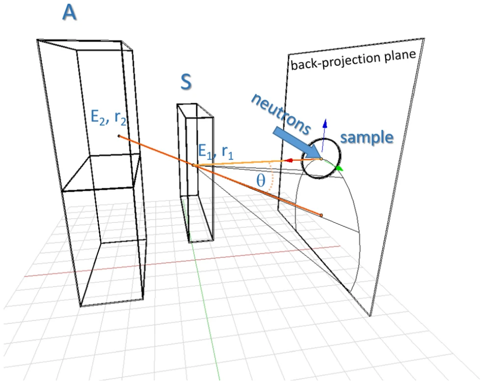

Figure 11: Back-projection of the Compton cone onto source plane.

FoM proposed

- **Figures of merit:**
  - Lambda
  - Angular Resolution Measure
  - Compton Angle
- **Experimental setup:**
  - Validation at different energies
  - Validation based on spatial or spatial-related information

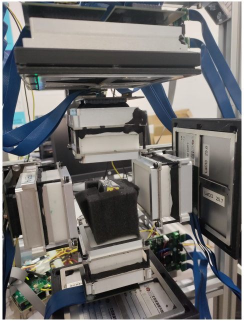

Figure 12: Experimental setup to study the background suppression applicability of different FoM. ^{22}Na source placed in front, side and back of i-TED-A module.

FoM proposed

- **Figures of merit:**
  - Lambda
  - Angular Resolution Measure
  - Compton Angle
- **Experimental setup:**
  - Validation at different energies
  - Validation based on spatial or spatial-related information

Figure 13: Experimental setup to study the background suppression applicability of different FoM. ^{22}Na source placed in front, side and back of i-TED-A module.

FoM proposed

- **Figures of merit:**
  - Lambda
  - Angular Resolution Measure
  - Compton Angle
- **Experimental setup:**
  - Validation at different energies
  - Validation based on spatial or spatial-related information

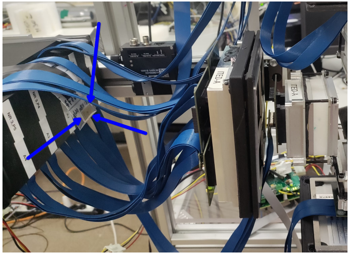

Figure 14: Experimental setup to study the background suppression applicability of different FoM. ^{22}Na source placed in front, side and back of i-TED-A module.

The ARM

- Angular difference between the Compton angle calculated assuming the source was in the center of the origin plane and the Compton angle calculated from the energies deposited

$$\mathrm{ARM} = \theta_{\mathrm{Position}} - \theta_{\mathrm{Energy}}$$
$$= \arccos\left(\frac{\vec{S}\cdot\vec{A}}{||S||||A||}\right) - \arccos\left(1 + \frac{m_{\mathrm{e}^-}}{E_T} - \frac{m_{\mathrm{e}^-}}{E_A}\right)$$

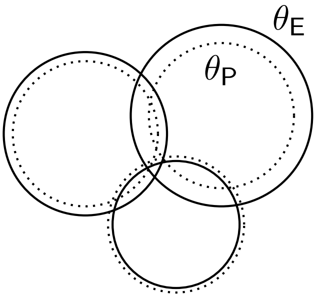

Figure 15: Definition of the Angular Resolution Measure.

The ARM

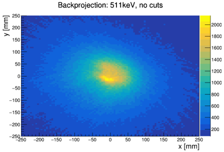

(a) Before cut

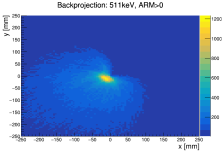

(b) After cut

Figure 16: Effect of ARM cut on imaging (3 pos).

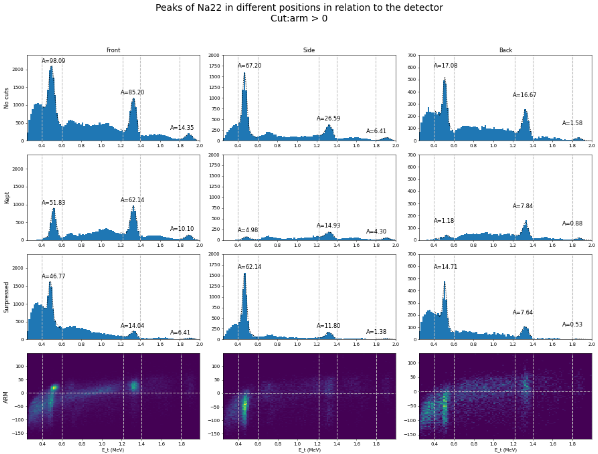

Figure 17: Effect of ARM cut on energy spectra.

The ARM

- **Method:**
  - 3 position of ^{22}Na
  - Normalized to less restrictive cut
  - Integral of peak over background spectrum taken
- **Result:**
  - Improved signal-to-background
  - Clear difference between the behavior of events spatially in front and in other positions

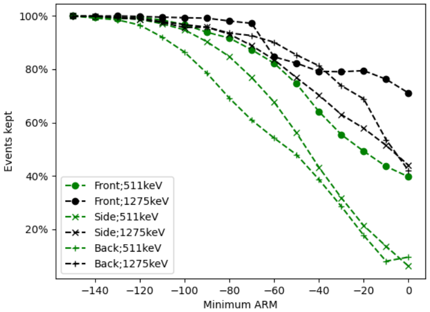

Figure 18: Restrictive cuts using the ARM FOM to suppress events based on spatial origin.

The Compton Angle

- It's the angle between the incoming and the outgoing γ-ray, defined by:

$$\cos\theta = 1 - \left(\frac{m_e c^2 E_s}{E_a E_t}\right)$$

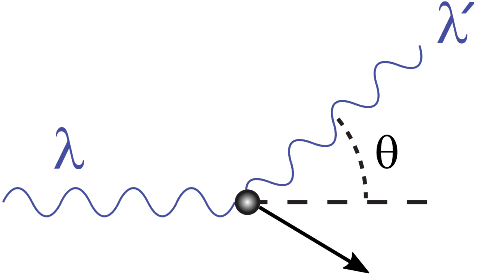

Figure 19: Definition of the Compton angle.

The Compton Angle

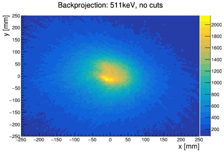

(a) Before cut

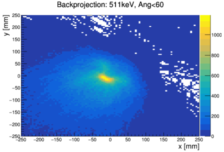

(b) After cut

Figure 20: Effect of Compton Angle cut on imaging (3 pos).

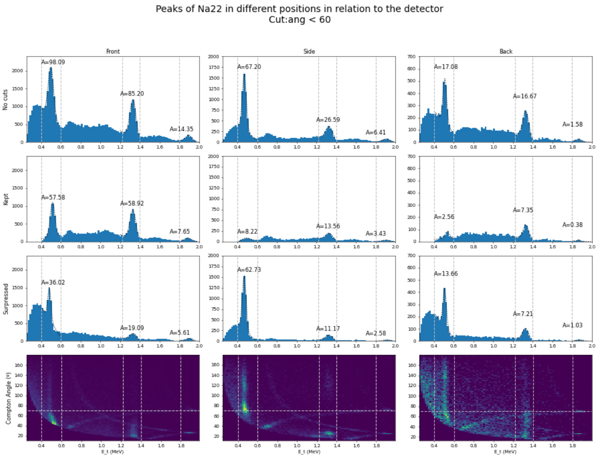

Figure 21: Effect of Compton Angle cut on energy spectra.

The Compton Angle

- **Method:**
  - 3 position of ^{22}Na
  - Normalized to less restrictive cut
  - Integral of peak over background spectrum taken
- **Result:**
  - Improved signal-to-background
  - Clear difference between the behavior of events spatially in front and in other positions

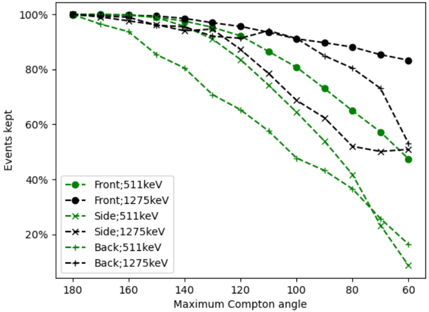

Figure 22: Restrictive cuts using the Compton Angle to suppress events based on spatial origin.

Outlook

- **Limitations:**
  - Experimental vs simulation
  - Impossible to completely classify good events
  - Having bad events as part of the data degrades the validation
- **Proposed:**
  - Monte Carlo simulation
  - Label the events properly
  - Study for more positions
  - Feature selection
  - Space selection
  - Study applicability of Machine Learning

Summary

- **i-TED modules:**
  - Multi i-TED array for astrophysics
  - i-TED-E for applications
  - Upgrades:
    - Per-pixel threshold
    - Thermal gain drift correction
    - CRT for PET mode
- **Imaging:**
  - Comparison of algorithms
  - Position sensitivity
  - Impact of focal distance
- **Suppression:**
  - Extended study of previous FoM
  - Two FoM that yield better results
  - Proposed future steps

Thank you!

- bgameiro@ific.uv.es
- hymnserc.ific.uv.es

- HYMNS-ERC Consolidator Grant
- ASFAE/2022/027

Event reconstruction

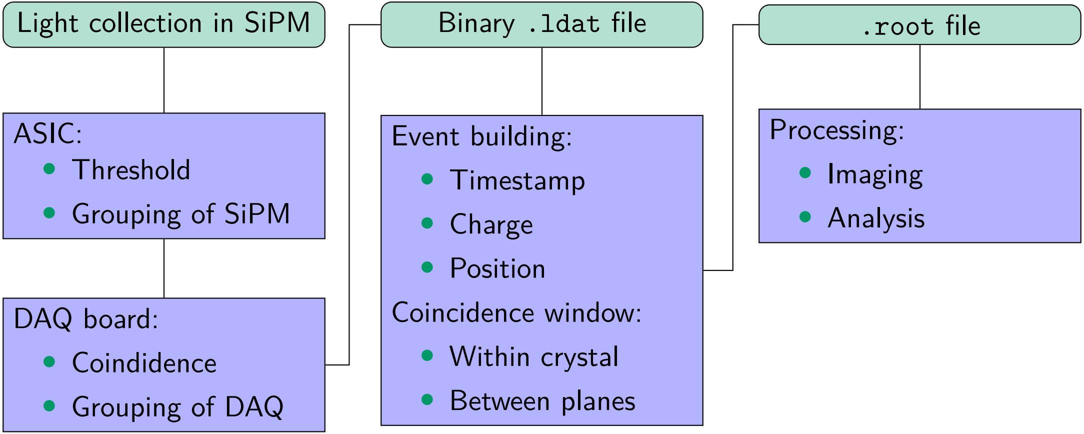

Figure 23: Simplified data pipeline for i-TED.

Problems & Upgrades: Minor

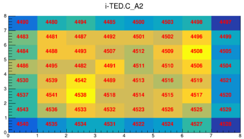

(a) Normal pixelmap

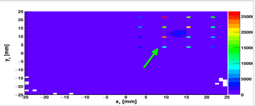

(b) Artifacts due to algorithm

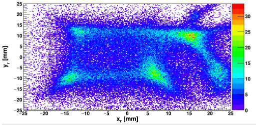

(c) Misreconstruction due to cloud in crystal

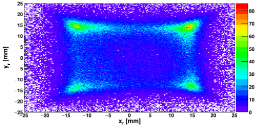

(d) Normal (compressed) position reconstruction

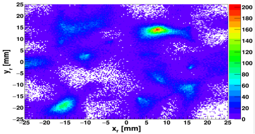

(e) Wrong pixelmap

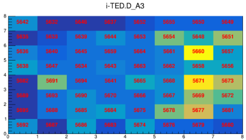

(f) Light

Problems & Upgrades: Major

Irregular pixelmaps

Noise from ≠ gains

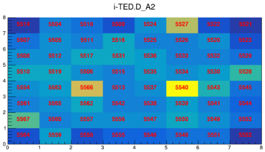

Per-pixel threshold

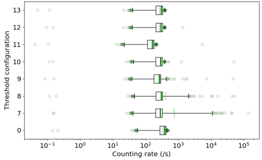

ASIC temperature

Thermal gain drift

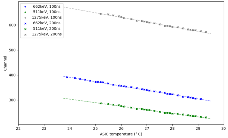

Temperature correction

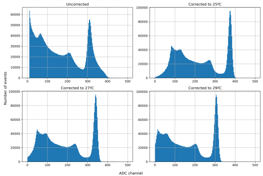

CRT study

PET mode

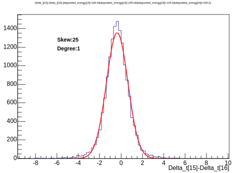

Compton mode

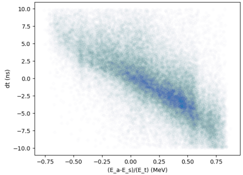

Problems & Upgrades: Software: Irregular pixelmaps

- Compromise needed?
  - ↑ Threshold
  - ↓ Noise
  - ↓ Energy resolution
- Per-pixel threshold!
  - How?
    - Per crystal
    - 5× median
  - Results
    - Resolution
    - File size

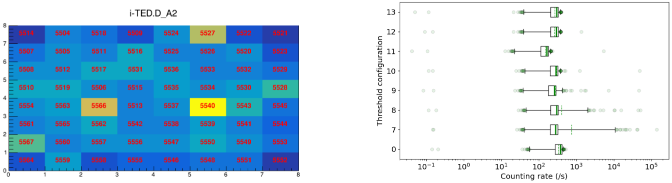

(g) Noisy pixels (h) Per-pixel threshold

Figure 24: Irregular pixelmaps.

Threshold	6	7	8	9	10	11	Custom
Size (MB/min)	2032	919	496	341	366	173	415

Table 2: Size of the text file `.singles.ldat` in 10^6 Bytes/min for different threshold parameters.

Problems & Upgrades: Software: ASIC temperature

- ASIC
  - Gain $\propto$ Temperature
  - $\beta \approx$-15ADC/°C
  - Function:

$$ADC_{\text{Ref}} = ADC_{\text{Measure}} + (T_{\text{Ref}} - T_{\text{Measure}}) \times \beta$$

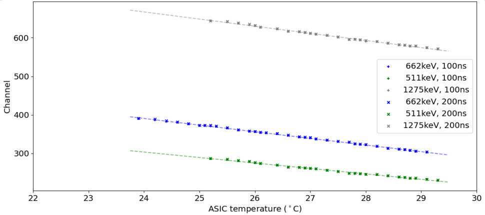

Figure 25: Thermal gain drift.

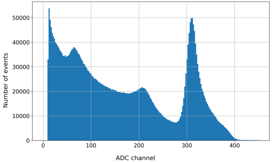

(a) Before

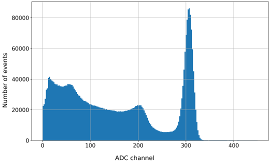

(b) After

Figure 26: Effect of thermal gain correction on spectrum.

Problems & Upgrades: Software: CRT study (PET mode)

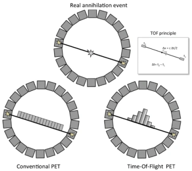

Figure 27: Illustration of PET and ToF PET.

- Calculate timestamp:

$$t_{\text{event}} = \frac{\sum_i^{min\{N_p,N_t\}} t_{\text{pixel}} \times E_i^W}{\sum_i^{min\{N_p,N_t\}} E_i^W}$$

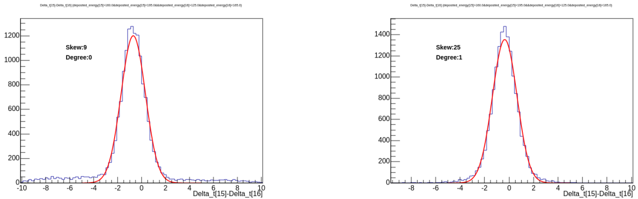

(a) $W = 0, N_p = 9$

(b) $W = 1, N_p = 25$

Figure 28: Best CRT configurations in PET mode.

(W, N_p)	(0,1)	(0,9)	(1,25)
FWHM (ns)	3.44	2.40	2.36

Table 3: FWHM time resolution in ns for coincidences between 2 crystals of i-TED-D using the two 511 keV γ-rays of ^{22}Na emitted at 180°.

Problems & Upgrades: Software: CRT study (Compton mode)

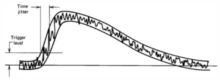

(a) Jitter

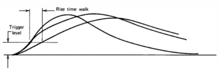

(b) Rise time walk

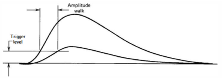

(c) Amplitude walk

Figure 29: Different phenomena and how they affect timing.

- Objective: $FWHM \leq \Delta t \approx \frac{2 \times 60mm}{299.8cm/ns} \approx 400ps$

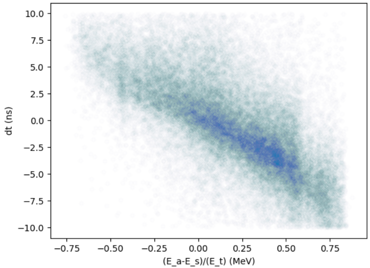

Figure 30: Time difference (ns) as a function of the difference between the deposited energies in absorber and scatter normalized to the total energy.

Characterization

Crystal spectrum

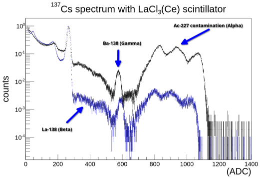

Figure 31: ^{137}Cs spectrum.

i-TED	A	B	C	D	Mean
Comparison	6.58±0.83	7.17±0.18	7.42±1.14	6.87±0.29	7.01±0.79
Best	6.28±0.70	6.90±0.20	6.92±0.90	6.75±0.48	6.71±0.67

Table 4: Mean resolution at 662 keV for each i-TED.

Add-back spectrum

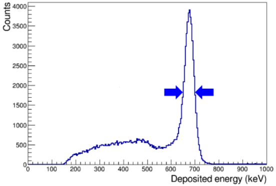

Figure 32: ^{137}Cs spectrum.

Absorber	1	2	3	4	Mean	All
Best	8.23±0.38	9.88±0.39	8.49±0.46	8.76±0.62	8.84±0.61	9.62±0.29

Table 5: Mean coincidence resolution at 662 keV for i-TED-A.

Focal

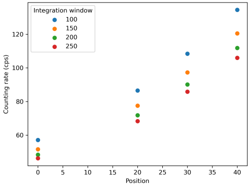

Figure 33: Counting rate in coincidence mode.

$$\text{Distance} = (75 - \text{Position})\ mm$$

Characterization

Crystal spectrum

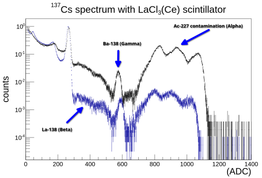

Figure 34: ^{137}Cs spectrum.

i-TED	A	B	C	D	Mean
Comparison	6.58±0.83	7.17±0.18	7.42±1.14	6.87±0.29	7.01±0.79
Best	6.28±0.70	6.90±0.20	6.92±0.90	6.75±0.48	6.71±0.67

Table 6: Mean resolution at 662 keV for each i-TED.

Add-back spectrum

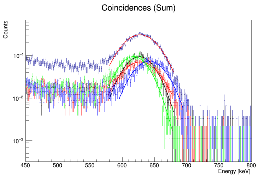

Figure 35: ^{137}Cs spectrum.

Absorber	1	2	3	4	Mean	All
Best	8.23±0.38	9.88±0.39	8.49±0.46	8.76±0.62	8.84±0.61	9.62±0.29

Table 7: Mean coincidence resolution at 662 keV for i-TED-A.

Focal

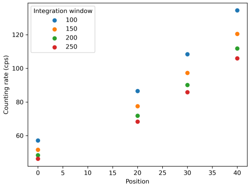

Figure 36: Counting rate in coincidence mode.

$$\text{Distance} = (75 - \text{Position})\ mm$$

Interactions of γ-rays with matter

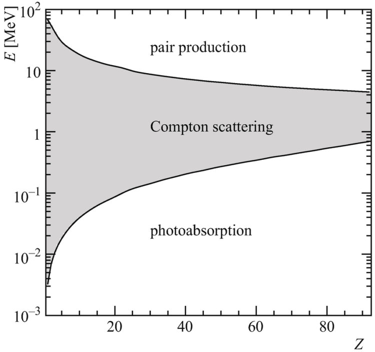

Figure 37: Interactions of electromagnetic radiation with matter.

Klein-Nishina

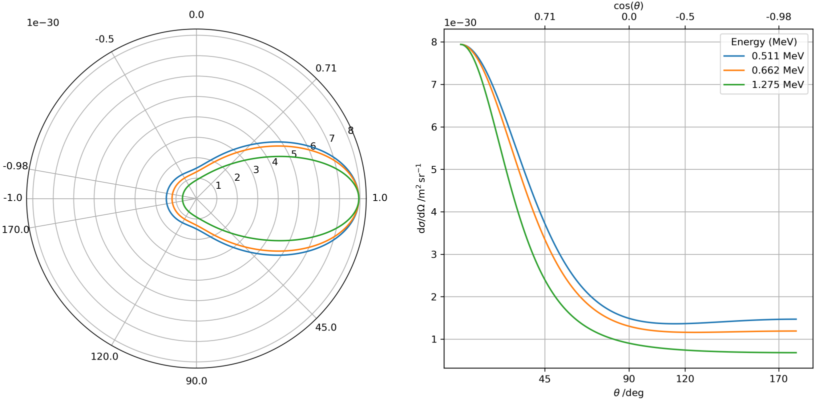

Figure 38: Scattering according to the formula of Klein-Nishina for several γ-ray energies that will be used in this work for the characterization of i-TED.

Intrinsic Activity of $LaCl_3(Ce)$

- **Intrinsic activity:**
  - β:
    - ^{138}La
    - Natural occurring
  - γ:
    - ^{138}Ba
    - Decays from ^{138}La
  - α:
    - ^{227}Ac
    - Contamination

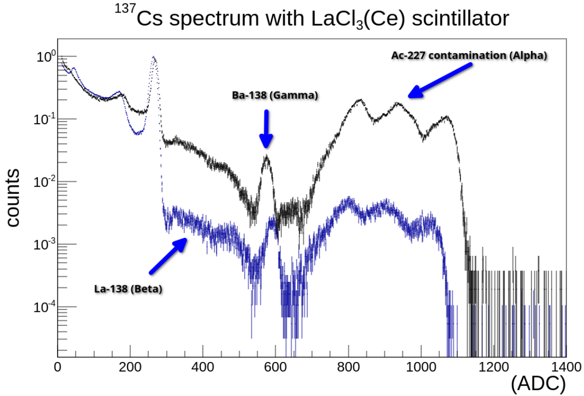

Figure 39: ^{137}Cs spectrum taken with a $LaCl_3(Ce)$ showing intrinsic activity.

Asymmetry after cut

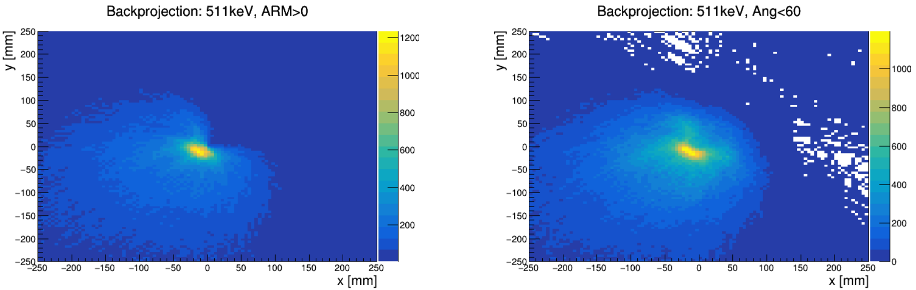

(a) ARM cut (b) Compton angle cut

Figure 40: Back-Projection images of ^{22}Na source with background after cuts.

Counting rate, not efficiency

- For a Compton camera, efficiency is a very complex topic
- In Compton mode, the efficiency of a given γ-ray depends on:
  - Energy
  - Distance to detector
  - Angle of position
  - Distance between planes
  - Different energy depositions in each plane

Previous study into Lambda FOM

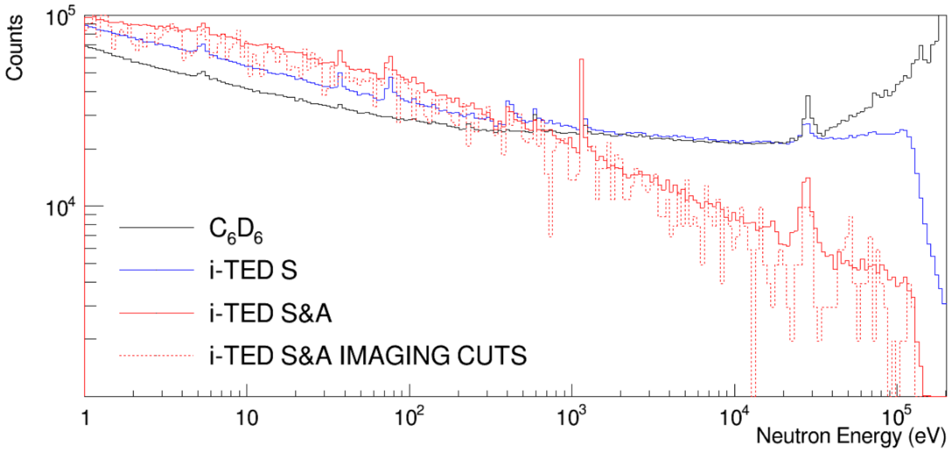

Figure 41: Neutron energy spectra measured with the ^{56}Fe sample using different detectors.

TOF detector

- **Characterization of neutron flux:**
  - Previous characterization:
    - TOF detector
    - Thin scintillator
    - Very fast response
  - During the experiment:
    - Neutron monitors
    - Validate flux
    - γ flash measured with main detector setup

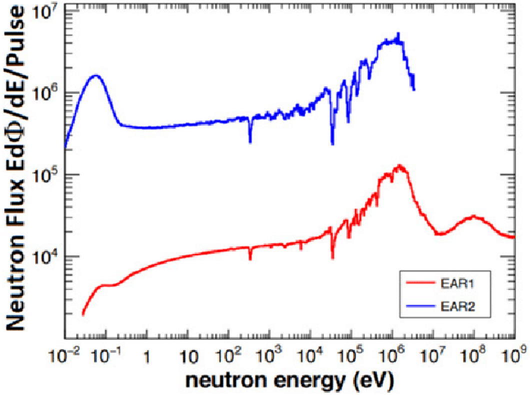

Figure 42: Neutron flux at both experimental areas of n_TOF.

n_TOF

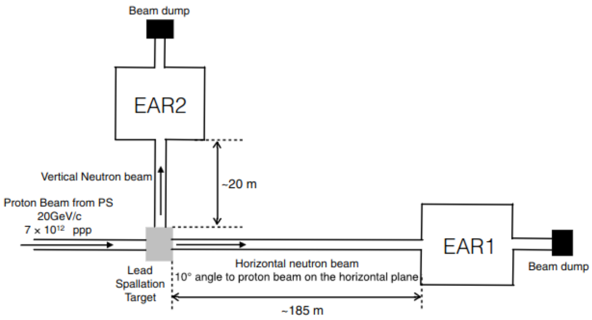

Figure 43: Effect of ARM cut on energy spectra.

Parallel single2trees

- Interaction reconstruction
- Created `.root` files from binary files
- New version with modularity in mind:
  - Data pipeline:
    - Prefect
  - Big data and distribution:
    - Dask
  - Performance:
    - Numba
    - Rapids
    - CuPy

Scientific Data Management

- Intake: Python module
- Data saved in YAML file
-
- Improvements:
  - Works regardless of file format
  - Adds metadata
  - Abstracts how to access files
  - Allows central data storage
  - Possibility of adding comments to measurement data

Calibration

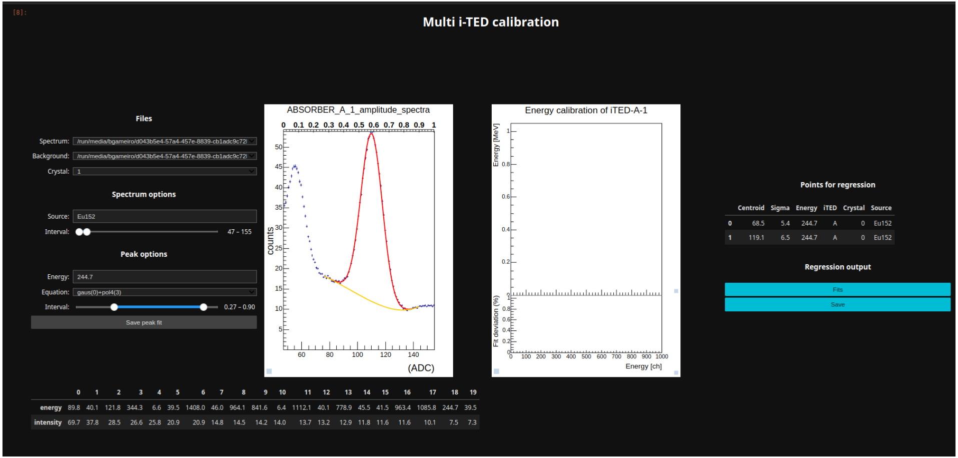

Figure 44: Calibration interface developed for i-TED.

Calibration

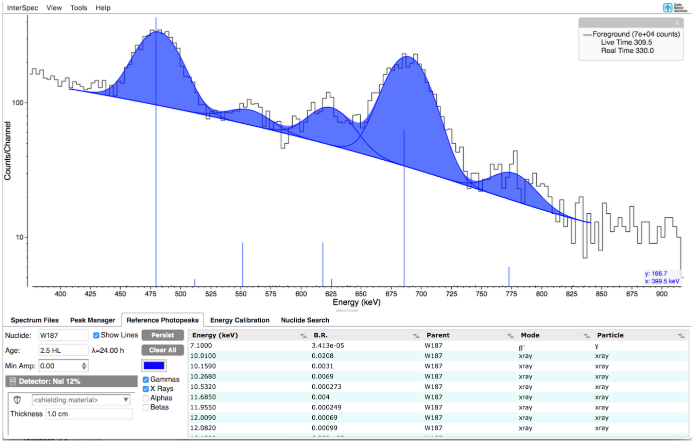

Figure 45: InterSpec calibration interface developed by SNL.

Analysis of suppression - ARM

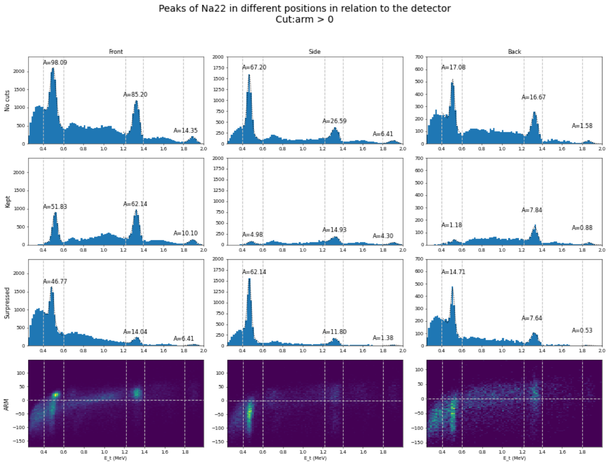

Figure 46: Effect of ARM cut on energy spectra.

Analysis of suppression - Compton Angle

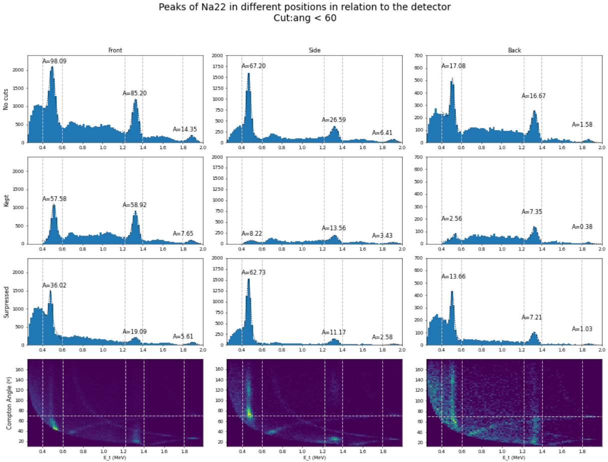

Figure 47: Effect of Compton Angle cut on energy spectra.

Range verification in hadrontherapy

- PET imaging widely used in medical physics
- PET vs Compton modes:
  - Compton can use different energy γ-rays
  - Compton has larger FOV
  - Compton uses prompt γ-rays that closely correlate to the Bragg peak
  - PET uses products of reactions that decay by β^+ and are subject to biological washup

Figure 48: Four i-TED modules during a study under clinical conditions at the Heidelberg Hadrontherapy Center.

Range verification in hadrontherapy

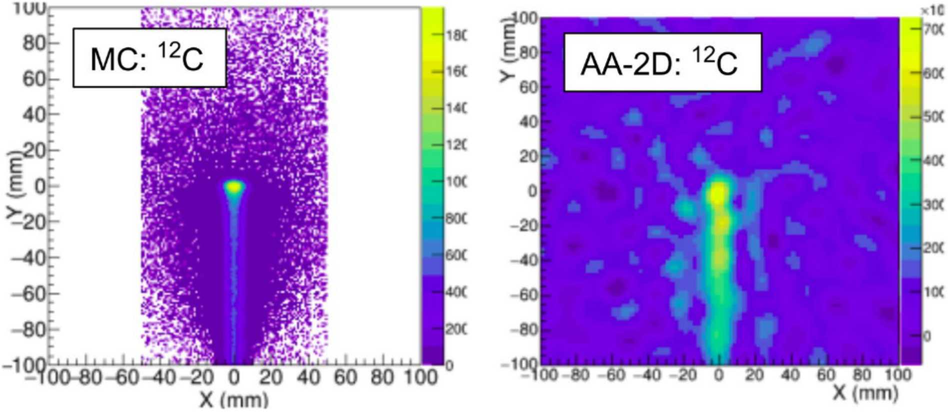

Figure 49: Monte Carlo simulation of proton beam depositing its energy in matter and corresponding Compton image of the emitted γ-rays.

GN-Vision

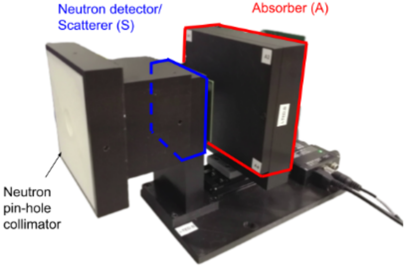

(a) GN-Vision

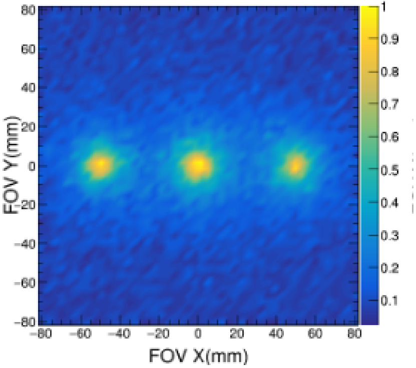

(b) Neutron imaging

Figure 50: GN-Vision: a Compton camera and neutron pin-hole imager.

Particle Identification

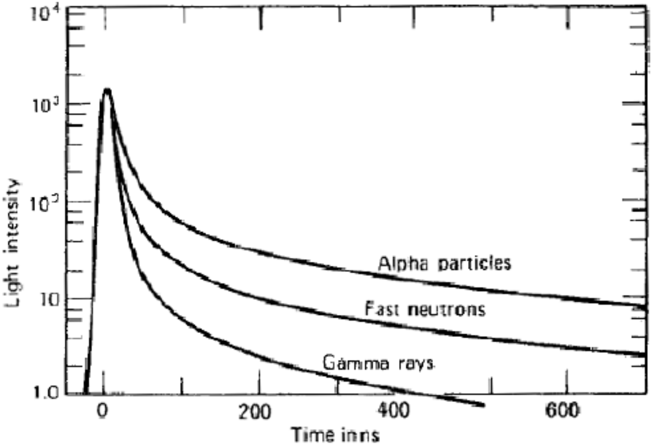

Figure 51: Pulse decay for different particles detected.

Particle Discrimination

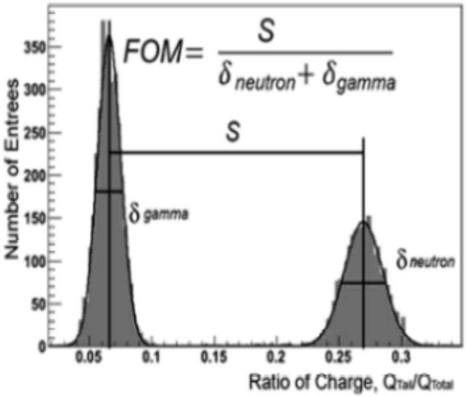

Figure 52: Visualization of the Figure of Merit in PSD

Scintillators

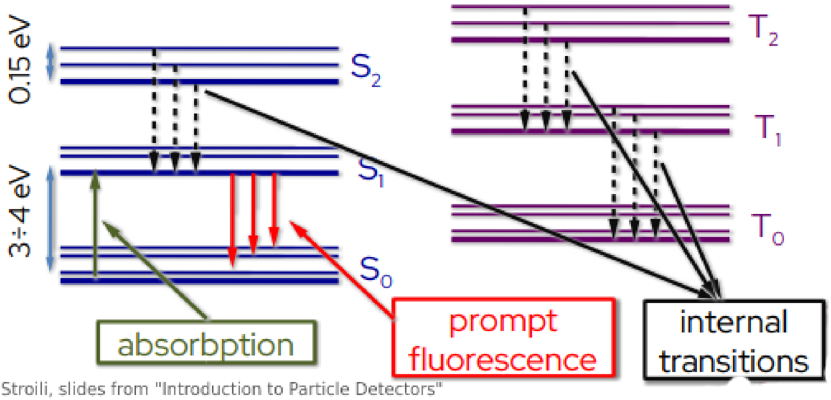

Figure 53: Scintillation: fluorescence or phosphorescence depending on the excited state